



Frame Transformation

Doc. Nr: GO-TN-HPF-GS-0193

Issue: 1.0

Date: 16.05.2007

Page: 1 of 22

GOCE High Level Processing Facility

Alternative method for rotation to TRF

Doc. No.: GO-TN-HPF-GS-0193

Issue: 1

Revision: 0

Date: 16 / 05 / 2007



Prepared by: The European GOCE Gravity Consortium
EGG-C



Document Information Sheet

Document Name
Alternative method for rotation to TRF

Document ID	Issue	Date
GP-TN-HPF-GS-0193	1.0	16/05/2007

Author	Institute
Johannes Bouman	SRON
Contributions from	Institute

Document Category	Document Class	Document Level
3	R	3

Configuration Item	Confidentiality Level
CI003	

Appropriate Signatures		
Name	Signature	Signature for approval
		NONE

Distribution List	
Person	Institute
R. Floberghagen, D. Muzi, C. Blacker, F. de la Feld	ESA/ESTEC
R. Rummel, T. Gruber	IAPG
R. Koop	SRON
EGG-c partners	

List	
DIL	NO
CDL	NO
CIDL	NO
CSL	NO
CCN	NO
SWPRL	NO

Data Package	
SRR	NO
ADIR	NO
CDR	NO
AR0	NO
AR 1	NO
AR 2	NO
BP CDR	NO
AR 3	NO



Frame Transformation

Doc. Nr: GO-TN-HPF-GS-0193

Issue: 1.0

Date: 16.05.2007

Page: 3 of 22

Document Change Record

ISSUE /REV.	CLASS (R=Review /A=Approval)	DATE	REASON FOR CHANGE	CHANGED PAGES / PARAGRAPHS
1.0	R	16/05/2007	New report that compares an alternative method for frame transformation with the baseline method implemented in V2 of the GOCE HPF	All

Table of Contents

1. INTRODUCTION	5
2. REFERENCES	5
3. THE ALTERNATIVE METHOD	6
4. NUMERICAL TESTS	7
4.1 MODEL GG IN GRF	7
4.2 BASELINE DATA	7
4.2.1 UNFILTERED GG	7
4.2.2 HIGH-PASS FILTERED GG	8
4.3 EIGEN-GLO4C	9
4.4 GOCE MODELS	10
4.4.1 SIGNAL FRAME TRANSFORMATION	10
4.4.2 ERROR PROPAGATION	12
4.5 COMPARISON WITH LSC IMPLEMENTATION	13
4.5.1 BASELINE METHOD	13
4.5.2 TIME DOMAIN AND ERROR PSD	14
4.5.3 GEOGRAPHICALLY CORRELATED ERRORS	17
5. CONCLUSIONS AND DISCUSSION	22

		<i>Frame Transformation</i> Doc. Nr: GO-TN-HPF-GS-0193 Issue: 1.0 Date: 16.05.2007 Page: 5 of 22
---	---	--

1. INTRODUCTION

In WP3000 LSC is used as the baseline method to predict all six GG's in the LNOF (EGG_TRF_2), given the four accurate GG's in the GRF (from EGG_NOM_2). To this end, the Earth is divided in blocks and in each block the transformation from GRF to LNOF is done. Besides the GOCE data, additional input needed is a pre-determined scaling of the signal covariance function in each block. The overall accuracy of the method seems to be good enough, that is, there is some degradation of GG accuracy in the MBW, but the final result is much better than for a direct point-wise rotation using all six GOCE GG's in the GRF, while the signal-to-noise ratio is well above one (Bouman et al., 2007).

Due to the signal covariance scaling, however, results may differ from block to block. In addition, the computational costs are high and EGG_NOM_2 needs a lot of additional post-processing (down-sampling to speed up computations, low-pass filtering to avoid aliasing, high-pass filtering and replacement below MBW with model gradients to allow LSC). An alternative method could be to replace V_{xy} and V_{yz} from EGG_NOM_2 by model gradients and do a direct points-wise rotation. Advantages may be that it is a computational low cost procedure and that EGG_NOM_2 may not need any further processing. Furthermore, no block-wise computations are necessary, so the EGG_TRF_2 accuracy could be geographically more homogeneous. A disadvantage could be that in the MBW GOCE and model gradients are mixed, which could lead to quality degradation in the MBW as compared to the LSC based method.

The purpose of this report is to assess the performance of the point-wise rotation as compared to the baseline method. Whether the alternative method will be used in the operational chain, depends on the trade-off between the GG accuracy in the MBW and the geographically correlated errors. This will be studied using ESA E2E Test Data.

2. REFERENCES

- [1] Arabelos, D., and Tscherning, C.C. (2003): Globally covering a-priori regional gravity covariance models, *Advances in Geosciences*, **1**, 143-147.
 - [2] Bouman, J., Rispens, S., and Koop, R. (2007): GOCE gravity gradients for use in Earth sciences, Proceedings of *The 3rd International GOCE User Workshop*, ESA-ESRIN, Frascati, Italy, 6-8 November 2006, ESA SP-627.
-

		<p><i>Frame Transformation</i> Doc. Nr: GO-TN-HPF-GS-0193 Issue: 1.0 Date: 16.05.2007 Page: 6 of 22</p>
---	---	---

3. THE ALTERNATIVE METHOD

A direct point-wise rotation of the GOCE GG from the GRF to the LNOF would project the larger GG error of V_{xy} and V_{yz} onto the other GG. The baseline GRF-LNOF transformation method in the GOCE HPF therefore uses the four accurate GOCE GG V_{xx} , V_{yy} , V_{zz} and V_{xz} in the GRF to predict with LSC all GG in the LNOF. A disadvantage of this method may be that it uses a pre-determined scaling of the signal covariance function in geographical blocks. This may lead to an inhomogeneous GG error in the LNOF, which could be undesirable.

An alternative method which would not have this disadvantage is a point-wise rotation with the GOCE V_{xy} and V_{yz} GG replaced by model GG. In addition, reference GG are subtracted in the GRF to minimize the signal, which may reduce the total error. The reference GG are added to the GG anomalies in the LNOF. Schematically this is shown below.

$$\begin{array}{ccc}
\text{GRF} & \left(\begin{array}{c} V_{xx}^{GOCE}, V_{yy}^{GOCE}, V_{zz}^{GOCE}, V_{xz}^{GOCE} \\ V_{xy}^{Model}, V_{yz}^{Model} \end{array} \right) - U_{ij}^{Ref,GRF} & \rightarrow T_{ij}^{GRF} \\
& \text{Point-wise rotation} & \downarrow \\
\text{LNOF} & V_{ij}^{LNOF} \leftarrow U_{ij}^{Ref,LNOF} + & T_{ij}^{LNOF}
\end{array}$$

In principle the model and reference gradients could differ, we will, however, let them be equal. Consequently, the anomalies for xy and yz are equal to zero in the GRF.

Because of the $1/f$ behavior of the GG error, leakage effects may occur. That is, as a result of the frame transformation, long wavelength errors in the GRF may leak to higher frequencies in the LNOF. We will therefore also study high-pass filtered data. The idea is to keep as much as possible the GOCE GG signal in the MBW, while the signal below the MBW is replaced with model GG signal. Symbolically, this is:

$$V_{ij}^{Comb} = V_{ij}^{Model} + HPF(V_{ij}^{GOCE}) - HPF(V_{ij}^{Model})$$

with $ij = xx, yy, zz, xz$. In the GRF-LNOF scheme above, the GOCE GG are replaced with the Combination GG. Consequently, the GG anomalies in the GRF will have no or little signal power below the MBW, while for the four accurate GG the original anomalous signal in the MBW and above is kept.

4. NUMERICAL TESTS

4.1 MODEL GG IN GRF

For the point-wise rotation we will use different model gradients to replace V_{xy} and V_{yz} . The baseline model is EGM96 complete to degree and order 360. EGG_IAQ_2c and SST_PSO_2i are used to derive the rotational information from LNOF to GRF and vice-versa. Because of the errors on EGG_IAQ_2c, the EGM96 model GG in the GRF are not errorless. EIGEN-GL04C and GOCE models from the AR-2 test are used as well.

4.2 BASELINE DATA

4.2.1 Unfiltered GG

As a first test we've used xy and yz model GG generated using EGM96. Because this gravity field model has been used in the generation of the GOCE GG simulated data, this is a baseline test. With the point-wise rotation of the unfiltered data, it will not be possible to obtain a smaller GG error in the LNOF using other model GG. We've used the first seven days of the E2E test data set. The GG errors in the LNOF are shown in Figure 1, blue lines. For reference the original GG error in the GRF are shown as well, red lines, where it should be noted that only for zz the two reference frames almost coincide. It is also for this gravity gradient that the error in the LNOF is at the same level as in the GRF. For the three other accurate GG, however, the accuracy in the LNOF is much worse for large parts of the MBW and below the MBW. This is probably caused by leakage of long wavelength errors to higher frequencies.

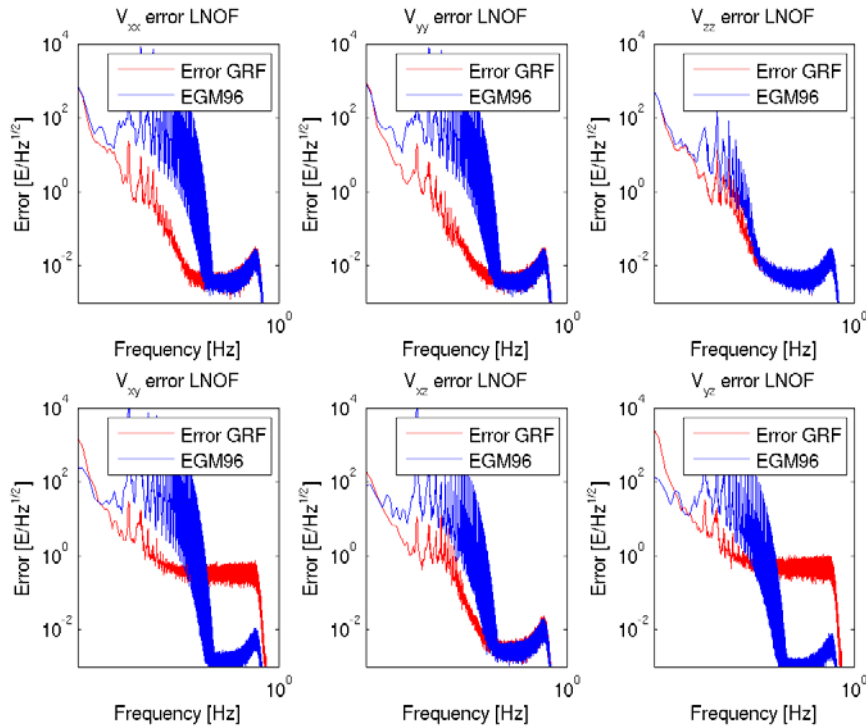


Figure 1: GG error PSD in LNOF using unfiltered data (blue line). The GOCE GG V_{xx} , V_{yy} , V_{zz} and V_{xz} have been used as well as EGM96 model GG V_{xy} and V_{yz} . For reference the GOCE GG errors in the GRF are shown (red line).

4.2.2 High-pass filtered GG

Obviously, the results with the unfiltered data are quite bad. We've therefore used a high-pass filter to suppress the long wavelength errors of the GOCE GG. We've used a 4th order high-pass Butterworth filter with a cut-off frequency of 5 mHz. The filter was applied in forward and reverse direction to remove any phase distortion, which in effect doubles the filter order. The GG signal at the low frequencies is replaced by model GG which have been filtered with the complementary filter. That is, for xx , yy , zz and xz

$$V_{ij}^{GRF,new} = HPF(V_{ij}^{GRF,GOCE}) + (1 - HPF)(V_{ij}^{GRF,model})$$

with HPF the high-pass filter. For the model GG we will use the same global gravity field model as for the xy and yz model GG.

In Figure 2 the error PSD's are shown for the filtered data (blue lines). The error in the LNOF in the MBW for the four accurate GG is now at the same level as the error in the MBW of the four accurate GG in the GRF. Below the MBW the error is of course low for low frequencies due to the replacement of signal at these frequencies by EGM96 model GG. The two less accurate GG show a spectacular error reduction in the LNOF as compared to the error in the GRF. The error RMS of the GG in the LNOF is summarized in Table 1.

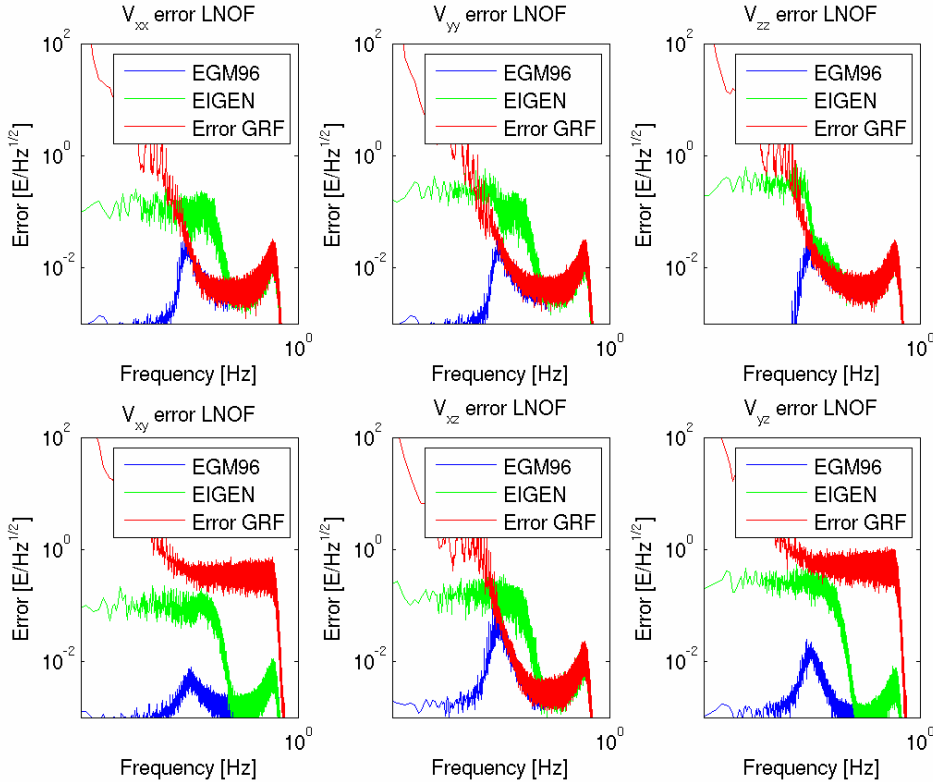


Figure 2: GG error PSD in LNOF using HPF data. The GOCE GG V_{xx} , V_{yy} , V_{zz} and V_{xz} have been used as well as EGM96 (blue line) or EIGEN-GL04C (green line) model GG V_{xy} and V_{yz} . For reference the GOCE GG errors in the GRF are shown as well (red line).

Table 1: RMS of GG errors [mE] in the LNOF after point-wise rotation from the GRF using GOCE high-pass filtered GG V_{xx} , V_{yy} , V_{zz} , V_{xz} and EGM96 model GG V_{xy} and V_{yz} .

	V_{xx}	V_{yy}	V_{zz}	V_{xy}	V_{xz}	V_{yz}
EGM96	5.9	5.9	6.4	2.3	4.6	1.7

For all other tests described below, the method with high-pass filtered data will be used.

4.3 EIGEN-GL04C

In reality we will of course not use the true xy and yz GG. We've therefore repeated the above tests using EIGEN-GL04C model gradients instead of EGM96. The EIGEN model was used complete to degree and order 360. In Table 2 the RMS of GG differences in the GRF between EGM96 and EIGEN are shown. In Figure 2 the error PSD's are shown, green lines. Except for zz , there is an error increase after frame transformation in the lower end of the MBW for the accurate GG. Also here the accuracy of the two less accurate GG in the GRF is higher in the LNOF.

Table 2: RMS of GG differences in mE between EGM96 and EIGEN-GL04C in the GRF.

	V_{xx}	V_{yy}	V_{zz}	V_{xy}	V_{xz}	V_{yz}
EIGEN	25.9	25.5	42.4	14.3	29.9	29.0

The RMS of the GG errors in the LNOF using EIGEN model GG is summarized in Table 3. Also shown are the results when the EIGEN model is used but with a lower maximum degree. It seems that the maximum degree is not of vital importance, but the errors tend to increase for a decreasing maximum degree. The corresponding error PSD's are shown in Figure 3. The differences between the different model GG are marginal.

Table 3: RMS of GG errors [mE] in the LNOF after point-wise rotation from the GRF using GOCE high-pass filtered GG V_{xx} , V_{yy} , V_{zz} , V_{xz} and EIGEN-GL04C model GG V_{xy} and V_{yz} .

	V_{xx}	V_{yy}	V_{zz}	V_{xy}	V_{xz}	V_{yz}
EGM96	5.9	5.9	6.4	2.3	4.6	1.7
EIGEN, L=360	13.3	16.8	17.6	11.6	16.2	24.7
EIGEN, L=200	13.3	16.8	17.6	11.6	16.2	24.7
EIGEN, L=100	13.8	17.2	17.7	13.5	17.0	28.6

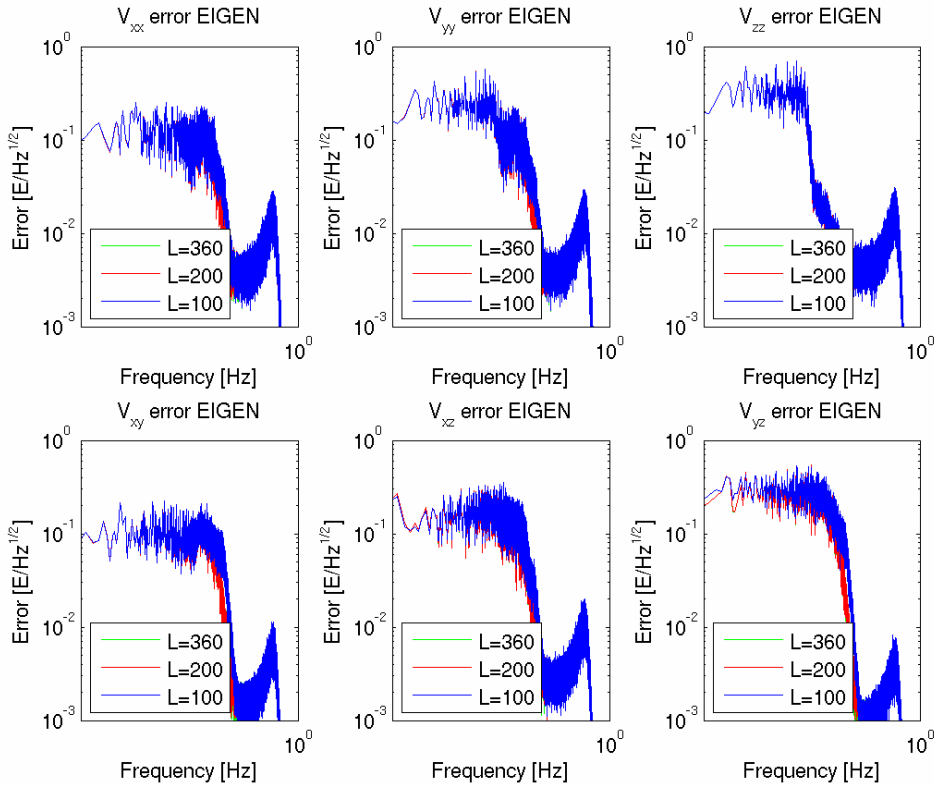


Figure 3: GG error PSD in LNOF using HPF data. The GOCE GG V_{xx} , V_{yy} , V_{zz} and V_{zx} have been used and EIGEN-GL04C model GG V_{xy} and V_{yz} complete to degree and order 360, 200 and 100 (green, red and blue line respectively).

4.4 GOCE MODELS

The E2E test data have been used by WP 5000, 6000 and 7000 to generate global gravity field models using the direct, time-wise and space-wise approach respectively. In addition, WP 6000 also produced a quick-look gravity field. As input the full set of two months of E2E data have been used, whereas for the quick-look gravity field almost four weeks of data were used. The GOCE orbits were assumed to be errorless, which may lead to too optimistic results at low frequencies.

4.4.1 Signal frame transformation

Table 4 lists the RMS of the GG differences between the model GG and EGM96 GG in the GRF (all using EGG_IAQ_2c, so these are the GG in the measured GRF). The GG error is at the same level for all four models, with a slightly larger error for the quick-look model. In Table 5 the RMS of the GG errors in the LNOF are shown. All models perform equally well and are as good as EGM96. Some difference in performance can be seen in the error PSD's which are shown in Figure 4 and Figure 5. The E2E data derived models have a larger error in the MBW than EGM96 for xy and yz , and there are some differences between the different models below the MBW. Overall, however, the performance of all four models is very satisfactory.

Table 4: RMS of GG differences in mE between GOCE models and EGM96 in the GRF.

	V_{xx}	V_{yy}	V_{zz}	V_{xy}	V_{xz}	V_{yz}
Direct	0.5	0.5	0.8	0.3	0.6	0.6
Space-wise	0.5	0.6	0.9	0.3	0.6	0.7
Time-Wise	0.5	0.6	0.8	0.3	0.6	1.0
Quick-look	0.6	0.7	1.0	0.4	0.8	1.5

Table 5: RMS of GG errors [mE] in the LNOF after point-wise rotation from the GRF using GOCE high-pass filtered GG V_{xx} , V_{yy} , V_{zz} , V_{xz} and GOCE model GG V_{xy} and V_{yz} .

	V_{xx}	V_{yy}	V_{zz}	V_{xy}	V_{xz}	V_{yz}
EGM96	5.9	5.9	6.4	2.3	4.6	1.7
Direct	5.9	5.9	6.4	2.3	4.6	1.8
Space-wise	5.9	5.9	6.4	2.3	4.6	1.8
Time-Wise	5.9	5.9	6.4	2.3	4.7	1.8
Quick-look	5.9	5.9	6.4	2.3	4.8	1.9

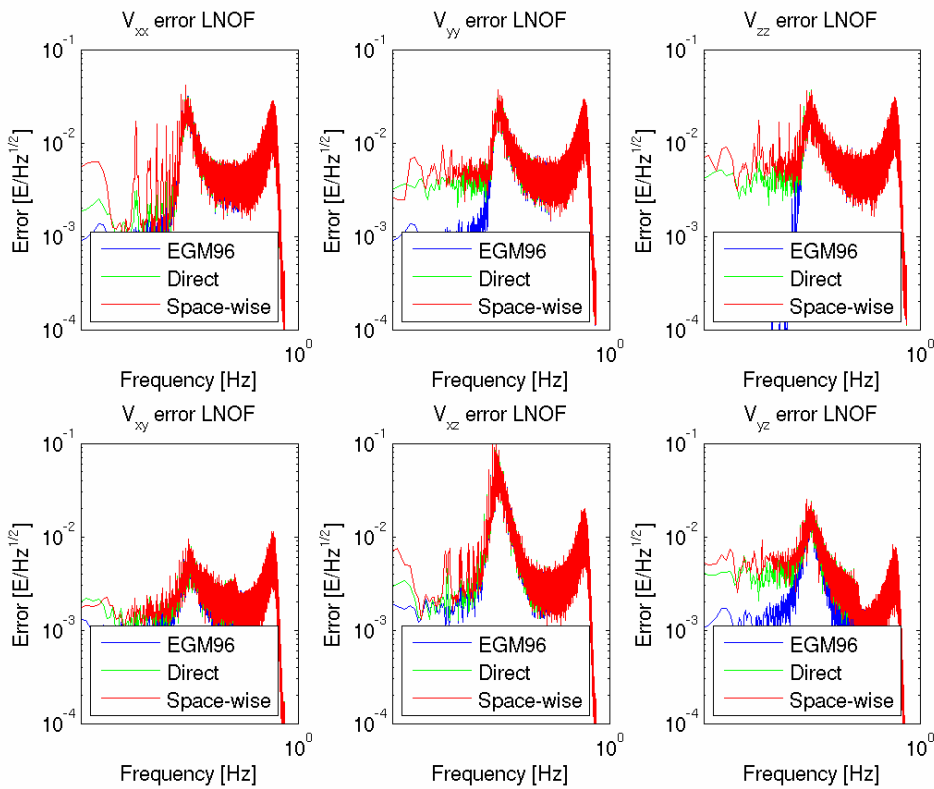


Figure 4: GG error PSD in LNOF using HPF data. The GOCE GG V_{xx} , V_{yy} , V_{zz} and V_{xz} have been used and model GG V_{xy} and V_{yz} (direct approach = green line, space-wise approach = red line).

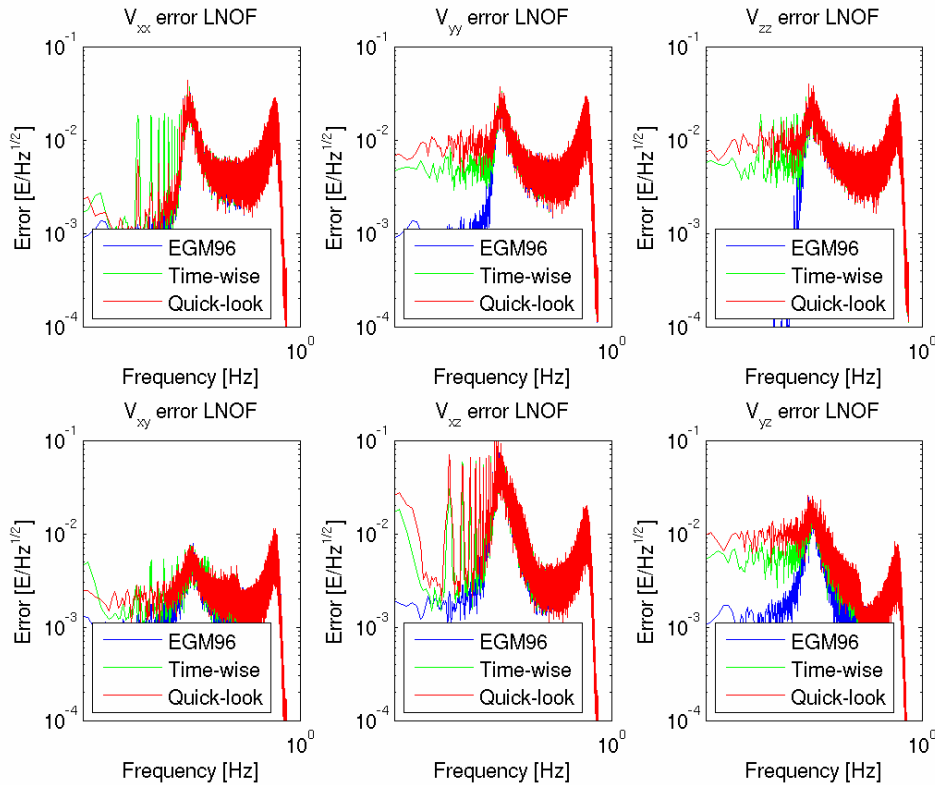


Figure 5: GG error PSD in LNOF using HPF data. The GOCE GG V_{xx} , V_{yy} , V_{zz} and V_{xz} have been used and model GG V_{xy} and V_{yz} (time-wise approach = green line, quick-look = red line).

4.4.2 Error propagation

Besides the GG in the LNOF also their formal errors are part of the EGG_TRF_2 product. In principle, the formal errors of EGG_NOM_2 after high-pass filtering for the accurate gravity gradients should be combined with the formal low frequency model errors for these gravity gradients, as well as the model errors for the two less accurate gravity gradients. These formal errors in the GRF should then be propagated to the LNOF. The error propagation is therefore not straightforward because of the use of filtered data. As an approximation one could consider to do an error prediction directly in the LNOF by using the model coefficient standard deviations.

The error prediction one would thus obtain, can only be valid in and below the MBW. The high frequency noise above the MBW requires a separate estimate. One option is to take the difference between the EGG_TRF_2 GG in the LNOF and the same GG to which a low-pass filter has been applied. This is shown in Table 6 (error above MBW does of course not change for different a priori gravity field models). A second option is to use an analytical approximation of the error above the MBW. For example, a reasonable fit for xx is a linear error increase with frequency above the MBW:

$$c \int_{0.1}^{0.4} f df = 5.3 \text{ mE}$$

where the constant c has been chosen such that at 0.1 Hz the error level is $7 \text{ mE/Hz}^{1/2}$. The first option is easy to implement and will be used here.

Table 6: RMS of GG errors [mE] in the LNOF above the MBW.

	V_{xx}	V_{yy}	V_{zz}	V_{xy}	V_{xz}	V_{yz}
All a priori models	5.6	5.6	6.1	2.2	4.0	1.5

In Table 7 the formal errors in the LNOF for the different models are shown, as well as sum of the formal errors and the errors above the MBW. With the exception of the quick-look model, the total error is determined by the error above the MBW. If we compare these errors with the “true” errors, Table 5, then we see that the predicted errors are close to the true errors, be it somewhat optimistic. For the quick-look model, the predicted errors are quite accurate for the GG that have a y-component. For the other GG the predicted errors are more pessimistic, approximately a factor of two larger than the true errors.

Table 7: Formal GG errors [mE] in the LNOF using error propagation.

	V_{xx}	V_{yy}	V_{zz}	V_{xy}	V_{xz}	V_{yz}
Formal error (quick-look)	10.7	0.8	10.9	0.8	10.8	1.1
Formal error + error > MBW	12.1	5.7	12.5	2.3	11.5	1.9
Formal error (direct)	0.2	0.3	0.4	0.1	0.2	0.3
Formal error + error > MBW	5.6	5.6	6.1	2.2	4.0	1.5
Formal error (space wise)	0.4	0.2	0.5	0.1	0.4	0.2
Formal error + error > MBW	5.6	5.6	6.1	2.2	4.0	1.5
Formal error (time wise)	0.2	0.3	0.4	0.1	0.2	0.3
Formal error + error > MBW	5.6	5.6	6.1	2.2	4.0	1.5

4.5 COMPARISON WITH LSC IMPLEMENTATION

4.5.1 Baseline method

The baseline method uses LSC to predict all six GG in the LNOF using as input the four accurate GG in the GRF. The idea is to do the prediction in each orbit point using the data of neighboring points. Initial tests indicated that for one month of data with homogeneous ground track coverage the prediction errors are small enough when the prediction is done in blocks of 6-by-6 degrees with 1.5 degree overlap. This serves two purposes. First, the limited number of data points in blocks limits the size of the system of equations to be solved. Secondly, LSC prediction performs best when the signal covariance function is regionally fitted [1]. We’ve determined a priori for each block the scaling of the signal covariance function using T_{zz} which was computed using EGM96 as gravity field model, degrees 61-360.

In practice we need to post-process EGG_NOM_2 before the data can be used in the frame transformation:

1. The computation time needed in GEOCOL increases approximately quadratically with the number of data points in each block. The computation time will be reduced when the data is down-sampled from 1 s to 5 s. This down-sampling is repeated four times, which gives 5 data sets (with a sampling of 5 s). After the rotation to the LNOF for each data set, the 5 LNOF data sets will be merged to restore the 1 s sampling. Because of the quadratic computation time increase with the number of data points,

the above scheme reduces the computation time with a factor of five¹ as compared to using the original 1 s data set.

2. The GG error tends to increase above the MBW, that is, above frequencies that correspond to 5 s sampling. Down-sampling from 1 s to 5 s would therefore lead to aliasing or the data needs to be low-pass filtered first. This filtering is justified because on the one hand the gravity field information at these frequencies is (far) below the noise in the data, while on the other hand the LSC prediction tends to smooth the data anyway. An 8th order low-pass Butterworth filter is used with a cut-off frequency of 0.2 Hz. The filter was applied in forward and reverse direction to remove any phase distortion, which in effect doubles the filter order.
3. Also here the long wavelength GG error may lead to a leakage type of effect. Therefore the GG from EGG_NOM_2 are high-pass filtered as well and the GG signal for these low frequencies is replaced by model GG which have been filtered with the complementary filter (see Chapter 4.2.2). The EIGEN-GL04C model is used to compute the model GG.
4. In the GRF model GG complete to degree and order L=60 are subtracted and the reference GG are later added in the LNOF (EIGEN-GL04C model gradients).

4.5.2 Time domain and error PSD

For the baseline method we've used one month of data in the computations. As in the preceding chapters, however, we will limit the analysis to the first week.

In Table 8 the error statistics are summarized for the baseline method (using LSC) and the alternative method (with QL model GG). Because the GG have been low-pass filtered in the baseline method, we also included the statistics for the alternative method when a LPF (low-pass filter) has been applied. That is, the GG in the LNOF are filtered with exactly the same LPF that has been used in the baseline method: an 8th order Butterworth filter with a cut-off frequency of 0.2 Hz, applied in forward and reverse direction.

Table 8: Statistics of GG differences [mE] in the LNOF after rotation from GRF (solution - true).

		V _{xx}	V _{yy}	V _{zz}	V _{xy}	V _{xz}	V _{yz}
LSC	Std	6.1	11.8	12.1	5.4	4.9	9.1
	Mean	0.2	0.1	-0.3	0.0	-0.2	0.0
	Max	61.8	135.0	83.3	51.3	77.0	99.0
	Min	-54.7	-86.8	-128.7	-44.4	-82.8	-89.0
QL	Std	5.9	5.9	6.4	2.3	4.8	1.9
	Mean	0.0	0.0	0.0	0.0	-0.1	0.0
	Max	26.8	27.8	29.1	17.8	23.0	18.6
	Min	-28.9	-29.8	-29.9	-17.5	-23.3	-19.9
QL, LPF	Std	1.6	1.7	1.9	0.7	2.6	1.2
	Mean	0.0	0.0	0.0	0.0	-0.1	0.0
	Max	9.6	11.4	17.5	7.4	12.6	10.3
	Min	-11.1	-11.1	-9.8	-4.6	-23.1	-8.1

¹ On our computer with the current implementation the wall-clock computation time is about 10 days for 1 month data.

The mean difference is (almost) zero for all cases, which is to be expected. The error standard deviation of the baseline method is always equal or larger than the error standard deviation of the alternative method. As compared to the filtered alternative method, the error standard deviation of the baseline method is two up to eight times larger. Also the minimum and maximum errors are much larger for the baseline method.

In Figure 6 time domain plots are shown of the GG errors in the LNOF. The larger noise level above the MBW of the alternative method without a LPF is clearly visible. It is also evident that the errors for the baseline method are inhomogeneous. For V_{xx} , for example, the error standard deviation is about equal for the unfiltered alternative method and the baseline method. While the error for the latter can be small for some regions, it is much larger elsewhere.

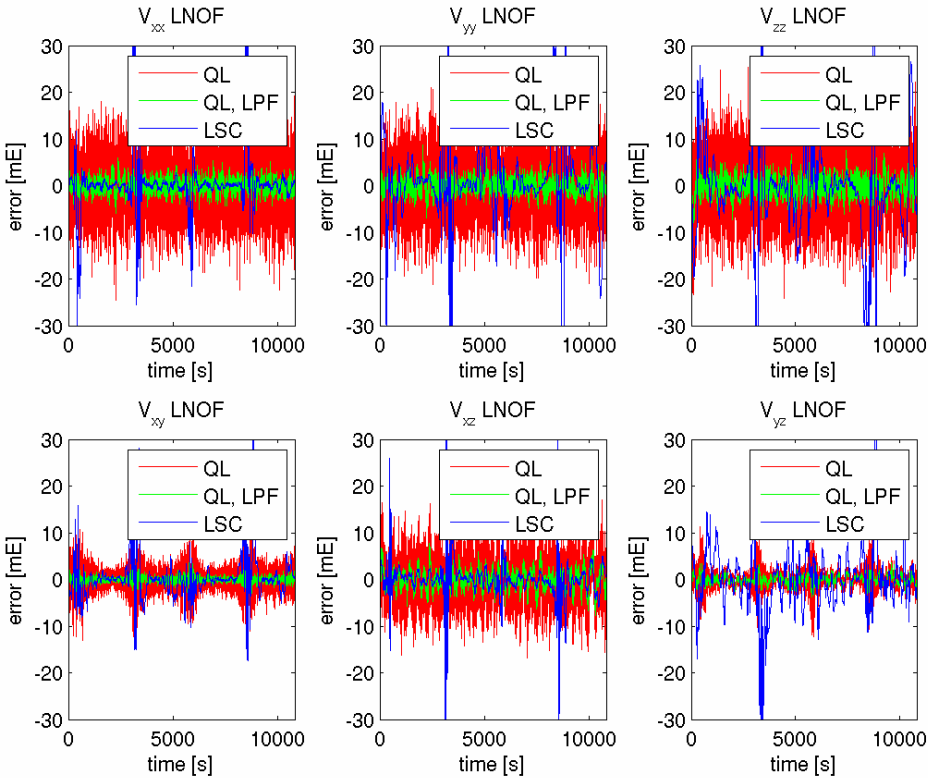


Figure 6: Time domain plots of the GG errors. The first two revolutions are shown.

Another feature of the baseline method is that discontinuities in the errors occur from time to time. As an example, see Figure 7 where the V_{xx} errors for the first 540 s are shown for the baseline method as well as the filtered alternative method. The errors for the other gradients show similar behavior. The discontinuities are a result of the pre-determined scaling per block of the signal covariance function. The use of smaller blocks and/or a more sophisticated regional adjustment of the signal covariance function may improve the results.

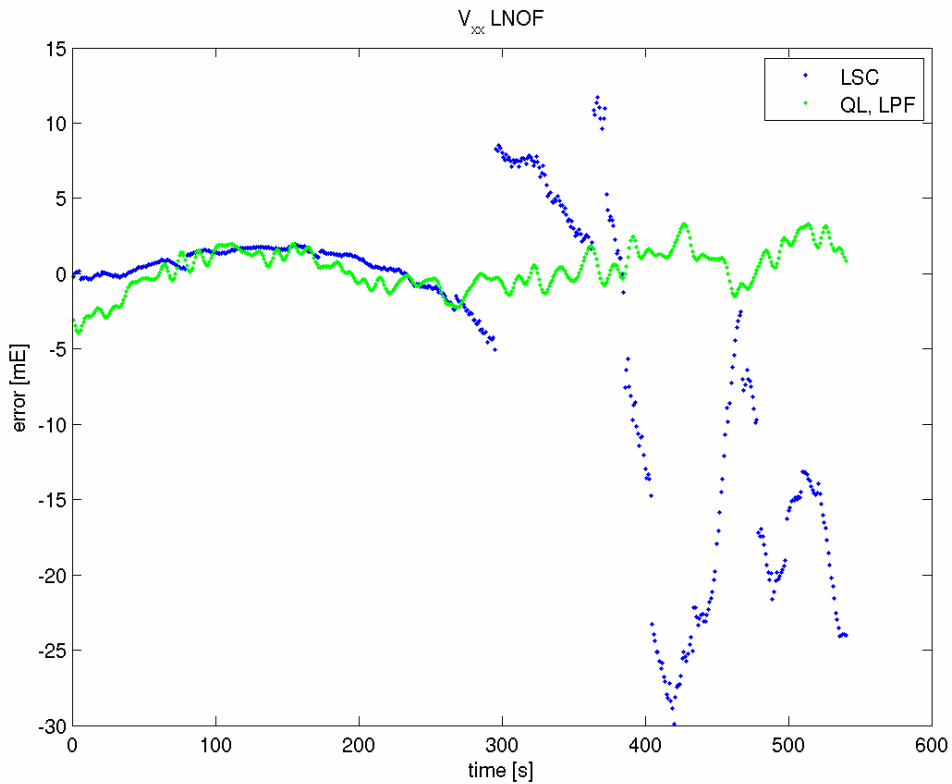


Figure 7: Time domain plots of V_{xx} errors. The first few hundred points are shown.

In Figure 8 the GG error PSD's for the baseline method as well as the alternative method are shown. Clearly, the errors for the baseline are larger than for the alternative method in and below the MBW. Besides the larger error standard deviation, the PSD plots for the baseline method also suffer from the discontinuities that were discussed earlier. Above the MBW, the baseline method gives smaller errors than the alternative method (no LPF), which is caused by the LPF and the inherent smoothing of the former method.

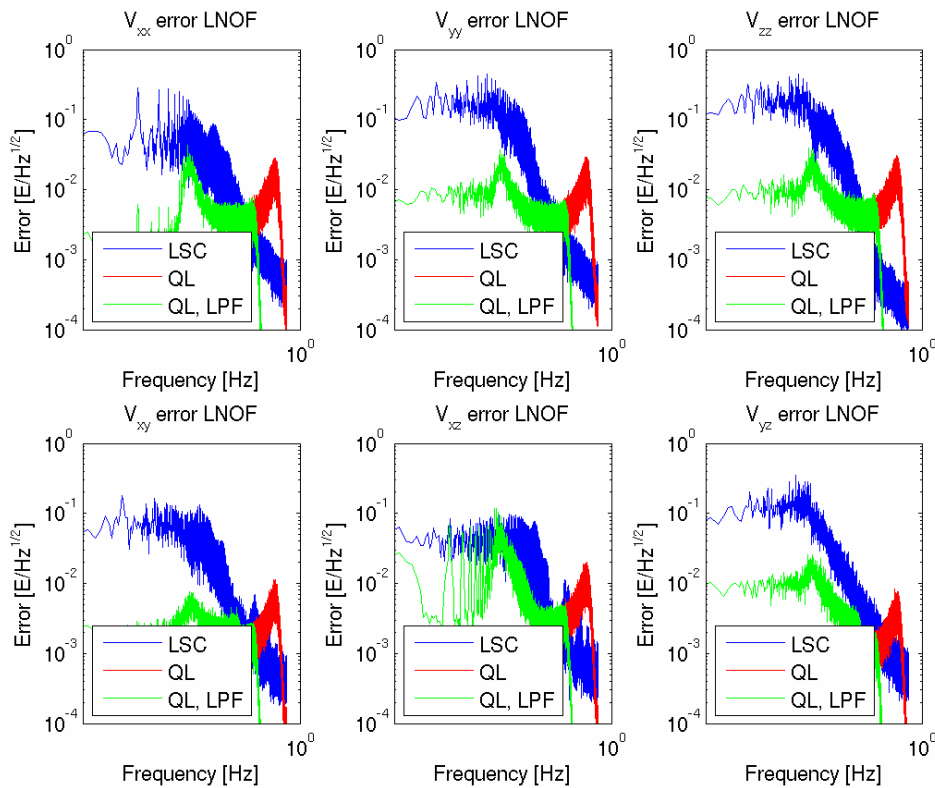


Figure 8: GG error PSD in LNOF for the baseline method and alternative method. The GOCE GG V_{xx} , V_{yy} , V_{zz} and V_{xz} have been used, while the alternative method also uses QL model GG V_{xy} and V_{yz} (baseline = blue line, alternative = red line, alternative low-pass filtered = green line).

4.5.3 Geographically correlated errors

In Figure 9, Figure 10, Figure 11 and Figure 12 the geographical correlated errors are shown for the baseline method as well as the alternative method, low-pass filtered. The errors for the baseline method seem to be correlated with the signal, that is, in regions such as Antarctica, South America, and the Himalayas the errors are large. For V_{xx} , in contrast, the errors are quite homogenous, apart from larger errors in the Polar Regions. This may be due to the fact that in the GRF this is the along track component, but it is not well understood. Another common feature is the appearance of more or less longitudinal bands around the Equator where the errors are equal. This is probably caused by the ground track distribution and the less dense cross track spacing near the Equator.

Also for the alternative method the longitudinal bands exist, while for the off-diagonal components the errors in the Polar Regions are somewhat larger. Also in this case the error seems to be correlated with the signal to some extent. However, the total error level is smaller than for the baseline method, see Table 8.

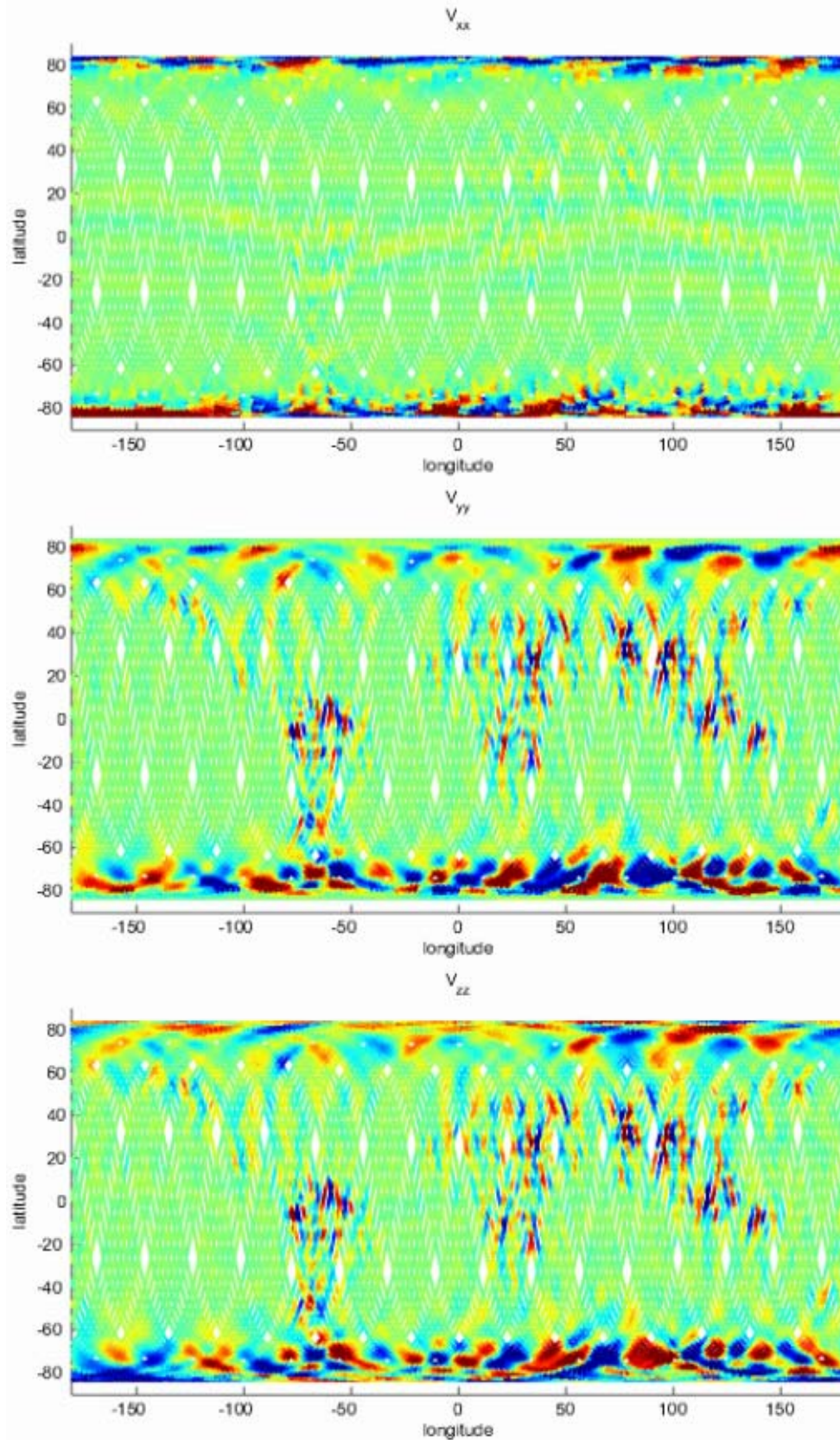


Figure 9: GG errors in LNOF (diagonal components), baseline method. Color scale has been set to $[-3\sigma, 3\sigma]$, see Table 8.

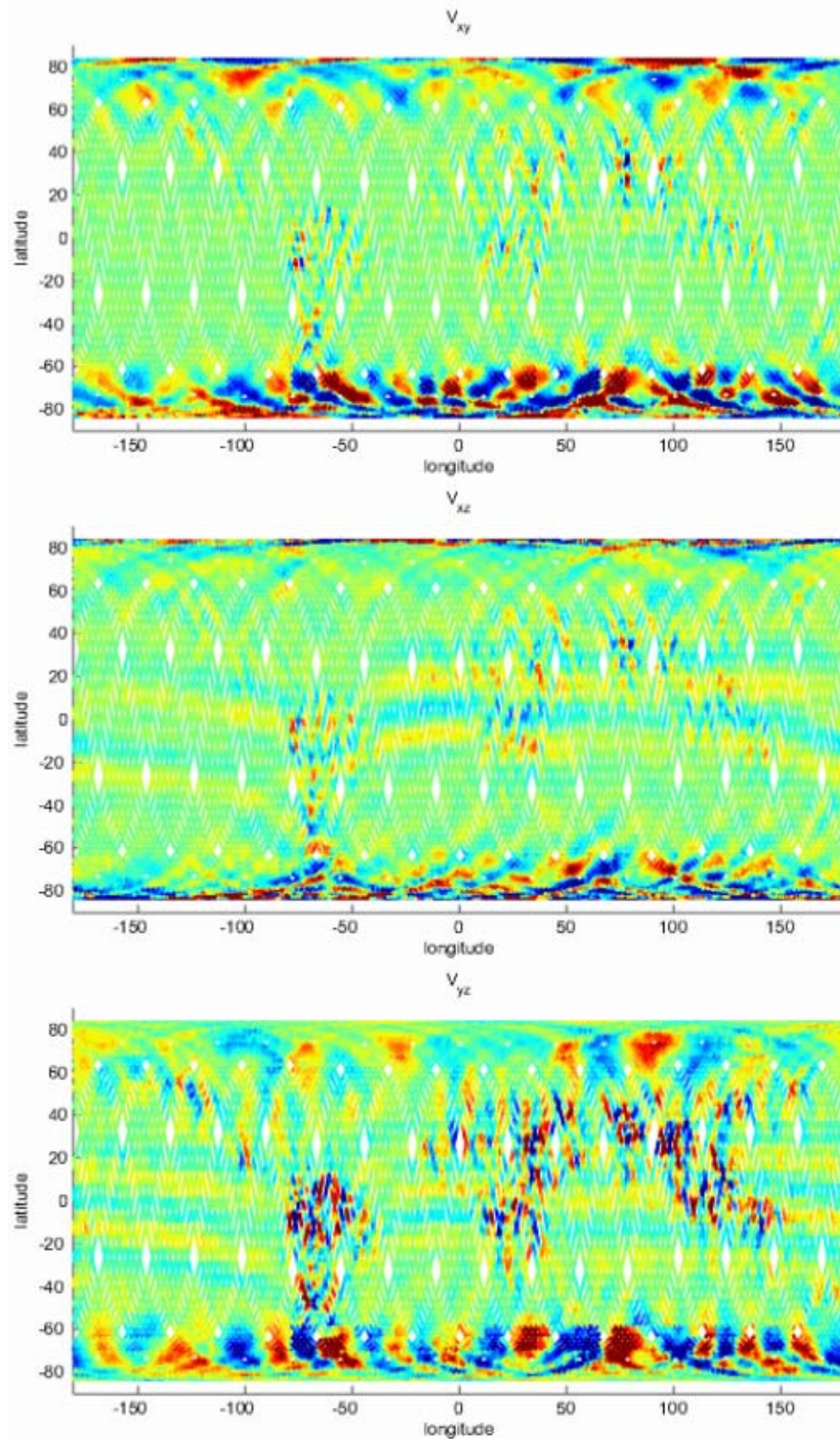


Figure 10: GG errors in LNOF (off-diagonal components), baseline method. Color scale has been set to $[-3\sigma, 3\sigma]$, see Table 8.

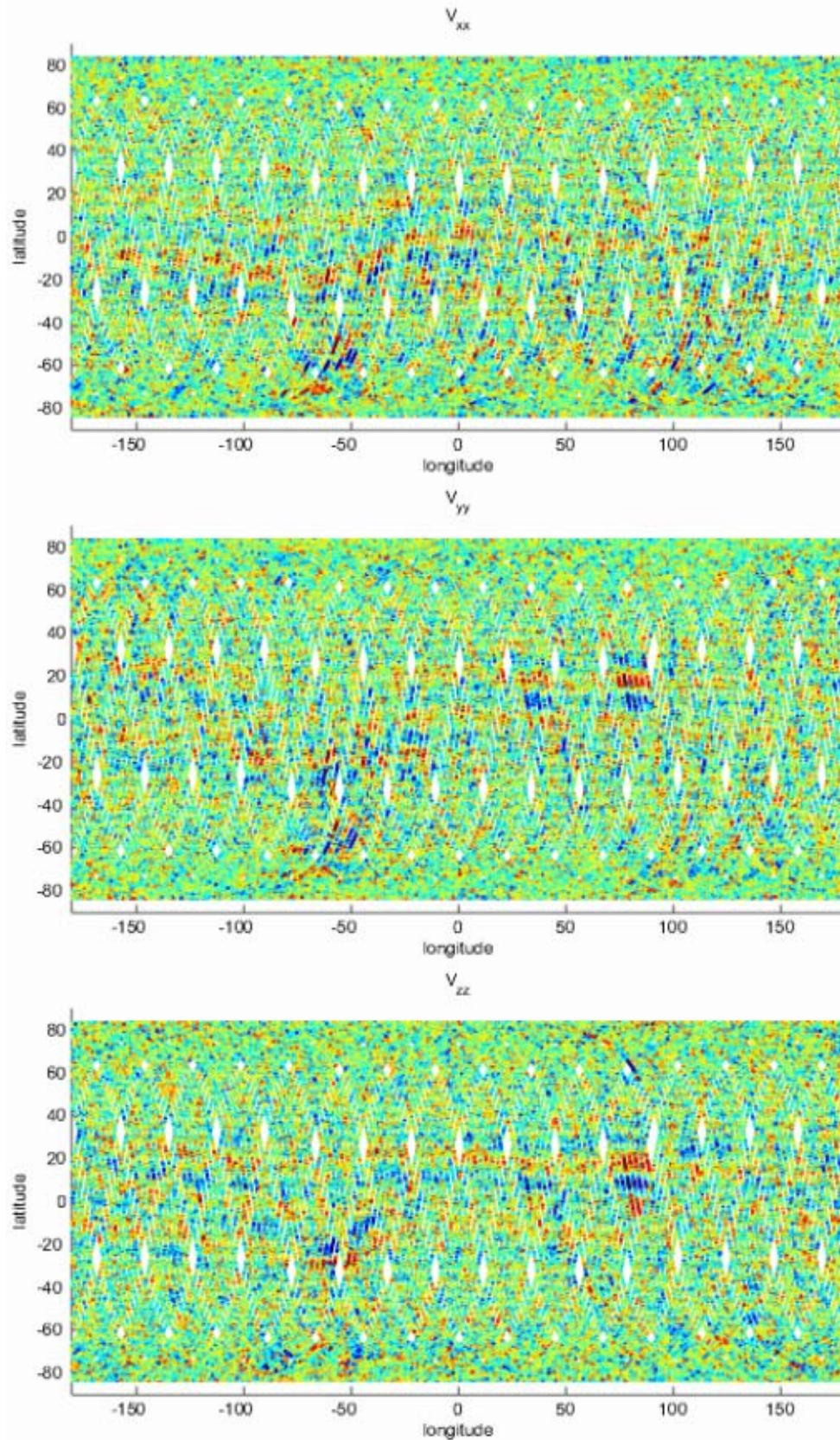


Figure 11: GG errors in LNOF after point-wise rotation (diagonal components, low-pass filtered). Color scale has been set to $[-3\sigma, 3\sigma]$, see Table 8.

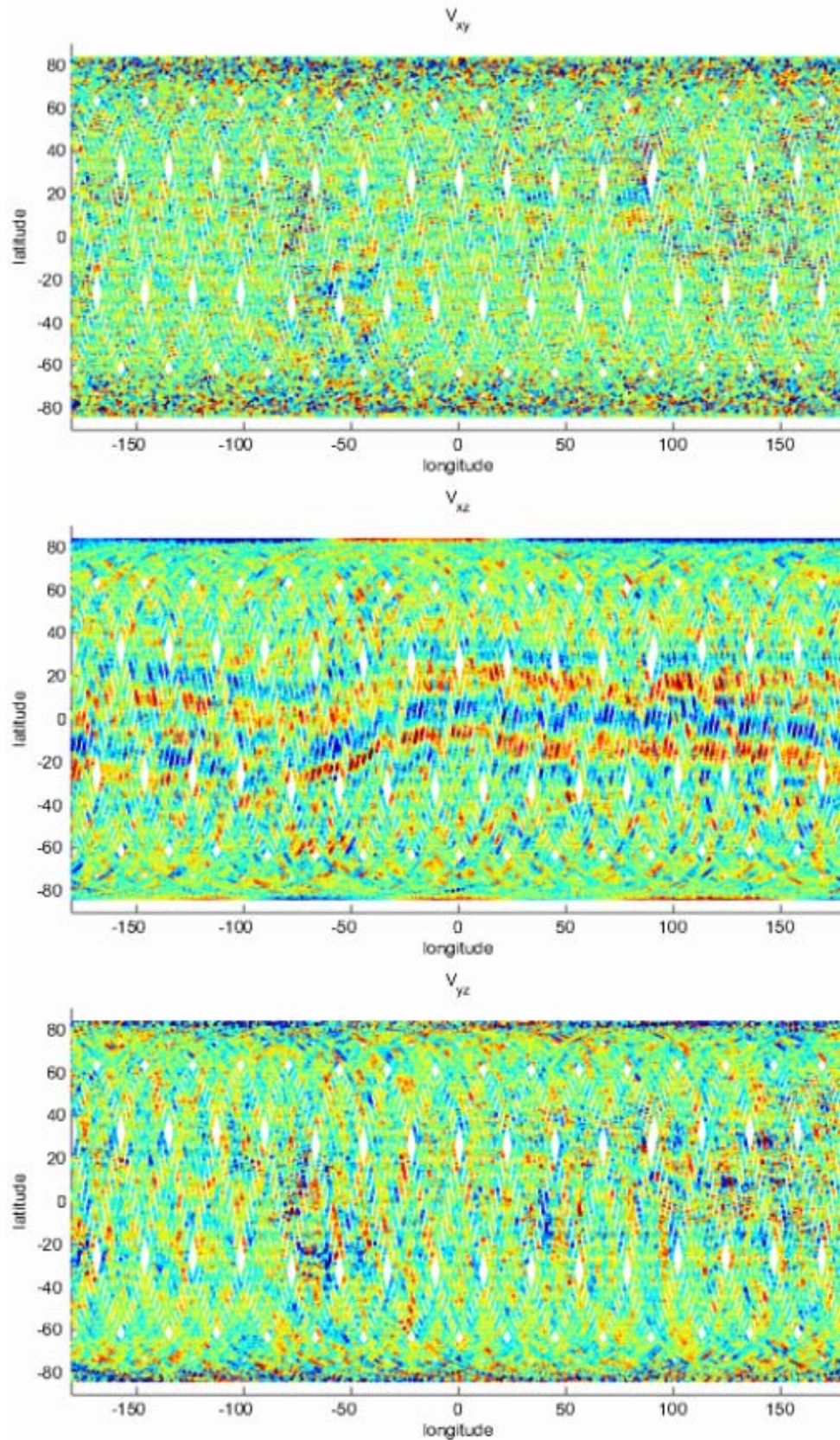


Figure 12: GG errors in LNOF after point-wise rotation (off-diagonal components, low-pass filtered). Color scale has been set to $[-3\sigma, 3\sigma]$, see Table 8.

		<p><i>Frame Transformation</i></p> <p>Doc. Nr: GO-TN-HPF-GS-0193</p> <p>Issue: 1.0</p> <p>Date: 16.05.2007</p> <p>Page: 22 of 22</p>
---	---	--

5.CONCLUSIONS AND DISCUSSION

- Point-wise rotation with GOCE QL V_{xy} and V_{yz} model GG performs better than the baseline method (in terms of computational costs and accuracy in the MBW of the GG in the LNOF). Both methods show geographically correlated errors and error – signal correlation, which is more pronounced for the baseline method.
 - Both methods require high-pass filtering to avoid leakage type of effects. That is, without HPF the long-wavelength errors in the GRF are projected onto higher frequencies in the LNOF.
 - The baseline method could be improved by using smaller blocks and/or the use of more advanced pre-determined regional covariance functions. The problem remains, however, that discontinuities between blocks may occur. Given the good performance of the alternative method it is also questionable whether it is worth the effort to try to improve the baseline method.
 - The alternative method using point-wise rotation should become the new baseline method.
 - The formal propagated error of the coefficients of the a priori gravity field model to GG in the LNOF, together with the error above the MBW, gives a reasonable approximation of the true error of the unfiltered GG EGG_TRF_2. The error above the MBW may dominate the total error.
-